Anisotropy of Pairwise Interactions between Hexadecanes in Water Measured by AFM Force Spectroscopy

ARTICLE *in* THE JOURNAL OF PHYSICAL CHEMISTRY C · OCTOBER 2008

Impact Factor: 4.77 · DOI: 10.1021/jp806580f

5 AUTHORS, INCLUDING:

Andrea Kirkpatrick
California Institute of Technology
9 PUBLICATIONS **274** CITATIONS

SEE PROFILE

Boris B Akhremitchev
Florida Institute of Technology
55 PUBLICATIONS **1,239** CITATIONS

SEE PROFILE

Anisotropy of Pairwise Interactions between Hexadecanes in Water Measured by AFM Force Spectroscopy

Chad Ray, Chao Gu, Jason R. Brown, Andrea Kirkpatrick[†], and Boris B. Akhremitchev[*]

Department of Chemistry, Duke University, Durham, NC 27708.

[*] e-mail: boris.a@duke.edu

RECEIVED DATE

TITLE RUNNING HEAD Anisotropy of hexadecane dimer dissociation

ABSTRACT. The pulling coordinate dependence of hexadecane dimer dissociation in water was studied using AFM-based single molecule force spectroscopy. Hexadecanes were covalently bound to both the AFM cantilever and to the glass substrates through hydrophilic poly-(ethylene glycol) tethers. The polymer tether was attached either to the end of hexadecane or in the middle of the molecule. Experimentally studied configurations of hexadecanes tethered to the AFM probe and to the glass substrate include a symmetric end-attached configuration (EE), an asymmetric end-attached vs. middle-attached configuration (ME), and a symmetric middle-attached configuration (MM). Kinetic parameters of the distance to the transition state barrier (barrier width) and activation energy of dissociation were extracted from the statistical analysis of double tether rupture events. The rupture force analysis

[†] Current address: Division of Chemistry and Chemical Engineering, California Institute of Technology, Pasadena, CA 91125.

employs a recently introduced two-bond model that corrects for errors induced by potential multiple simultaneous rupture events and accounts for the tether stiffening effects. Effects of the shape of intermolecular potential were considered by using the Bell-Evans and Hummer-Szabo force spectroscopy models. The activation energies to dissociation were similar for all configurations while the barrier width was significantly shorter for the MM and ME configurations than for EE configurations. Primitive models that include touching or merging spherical or cylindrical shapes were considered. These models were inconsistent with the extracted kinetic parameters. It is suggested that the observed anisotropy may be a result of conformational transition of hexadecane from extended to collapsed state during dimerization. A flexible four-bead model of hexadecane was introduced to account for conformational flexibility. Using the length and solvent accessible surface area of hexadecane, the four-bead model gave molecular dissociation parameters consistent with the experimental data. This suggests that conformational flexibility is an important factor in hydrophobic interactions between alkane chains.

KEYWORDS. hydrophobic interactions; hexadecane; hydrocarbons; alkane conformations; single-molecule; two-bond rupture; surfactants; self-assembly ; force spectroscopy; pulling direction

I. Introduction

This paper considers effects of the pulling direction on forced dissociation of a simple, yet geometrically complex, dimer of hydrophobic alkane molecules. External force applied to a molecular bond tilts the potential energy landscape, directing the course of the reaction.[1,2] Recent protein unfolding experiments and simulations have demonstrated that mechanical properties of globular proteins under applied force depend on the direction of force.[3-6] The kinetics of protein unfolding under applied force significantly varies with the direction of applied force.[4,6] A simulation that uses relatively simple protein folds indicates that by varying pulling direction molecular-level insights of protein molecule stability can be gained.[5] Linear alkanes represent a simple yet anisotropic system where changes in the pulling direction can be used to quantify the potential of mean force of hydrophobic

molecular bonds in different coordinates. Pulling coordinate effects can be measured by relocating the attachment point on the alkane molecule that is used for covalent immobilization of alkanes.

The size and geometry of associating non-polar solutes affect the energetics of hydrophobic attraction.[7-13] Typically, the potential of mean force (pmf) is calculated for symmetric non-polar molecules [14-18] or for a particular orientation between hydrophobic molecules, [9,19,20] or average all orientations.[13] Calculated one-dimensional pmfs can be compared to the kinetic parameters measured using force spectroscopy.[1,21] Kinetic parameters typically extracted from force spectroscopy measurements include the distance to the transition state $x^{\ddagger}$ (henceforth called the barrier width for brevity), dissociation rate extrapolated to the zero pulling force k_0 and the activation energy of dissociation $\Delta G^{\ddagger}$. Simulation results are available for small molecules, methane-like molecules and alkanes as large as neopentane, giving remarkably similar barrier widths ($x^{\ddagger}$ = 0.15-0.2 nm) and noticeably varied activation energies of dissociation ($\Delta G^{\ddagger}$ = 3-14 kJ/mol).[15-18] For small conformationally rigid molecules the free energy of the transition state $G^{\ddagger}$ can be significant in comparison to the thermodynamic energy of dissociation. Some results from larger hydrophobic polypeptide chains in fixed α-helical conformations $Alanine_{20}$ and $Leucine_{20}$, are also available, with noticeably different pmfs (Ala_{20}: $x^{\ddagger}$ = 0.24 nm, $\Delta G^{\ddagger}$ = 68 kJ/mol; Leu_{20}: $x^{\ddagger}$ = 0.6 nm, $\Delta G^{\ddagger}$ = 165 kJ/mol).[20] Ala_{20} shows a small activation barrier to dimerization (~8 kJ/mol) while Leu_{20} shows no activation barrier to dimerization. Recent experimental results for alkanes from dodecane to octadecane have shown barrier widths at the higher end of the range of simulation data ($x^{\ddagger}$ = 0.55-0.97 nm, $\Delta G^{\ddagger}$ = 44-51 kJ/mol).[22] Explicit solvent simulations of three methane pmf indicate that there is a noticeable dependence in the activation energy and in the distance between the minimum energy state and the transition state ($x^{\ddagger}$) on a polar angle between methane dimer C_{∞} axis and the direction of the third methane approach.[23] However, previous experimental studies did not consider possible directional dependence of kinetic parameters. This dependence may be expected even for simple alkane associations.[7] Moreover, conformational transition of alkane chains during dimerization [22] might be manifested in the pulling direction dependence of kinetic parameters.

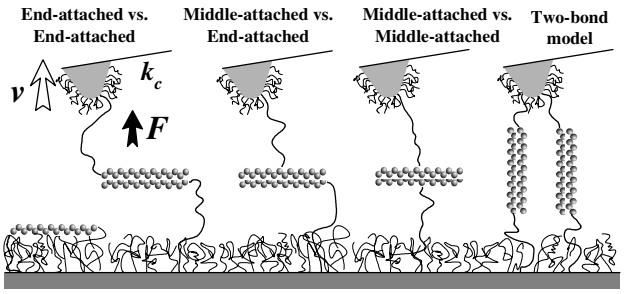

Figure 1. Cartoon representation of the three attachment points used here. The symmetric and asymmetric end-attachment and middle-attachment of hexadecane are used in dimer dissociation experiments.

Here we investigate the pulling direction dependence directly using a single-molecule force spectroscopy technique that has been used previously to quantify interactions between individual hydrophobic molecules.[22,24-26] The developed experimental methodology facilitates measurements of interactions between the test molecules using the double-tether approach and addresses possible systematic errors in the measured kinetic parameters. [26-28]

In our experiments, alkane molecules are covalently tethered via hydrophilic poly-(ethylene glycol) (PEG) linkers to the glass substrate and to the probe of an atomic force microscope (AFM) through attachment points at the end and in the center of the molecule. This double-tether approach facilitates single-molecule measurements and removes spurious surface effects. [24,25,29] Both symmetric pairs (end-attachment vs. end-attachment, denoted EE, and middle-attached vs. middle-attached, denoted MM) and asymmetric pairs (middle-attached vs. end-attached, denoted ME) have been studied, as illustrated in Figure 1.

It was noted previously that force spectroscopy results can be biased by employing a particular theoretical model for the data analysis. [21,26-28,30] In the data analysis employed here we explicitly consider the effects of tether stiffening, shape of the intermolecular potential, and the contribution of multiple simultaneous rupture events. [26-28] The two-bond model [28] is used to fit the rate-dependent distributions of rupture forces and extract kinetic parameters corrected for the identified systematic errors. The resulting kinetic parameters are compared to the values obtained from simple geometrical

models of hexadecane association. The results indicate that the measured pulling direction anisotropy of pairwise hydrophobic interactions between hexadecanes in water is consistent with collapse of extended monomers into a globular state upon dimerization.

II. Experimental Details

II-a. Instrumentation and Materials. Force spectroscopy was carried out using an Asylum Research Molecular Force Probe 3D AFM (Santa Barbara, CA). Glass microscope cover slips (Fisher Scientific) were used as substrate opposite commercial AFM cantilevers (Veeco, model NP). Measurements were performed in pH 7 phosphate buffer (VWR International, contains: disodium hydrogenphosphate and potassium dihydrogenphosphate, 0.05 M). NMR spectra were collected on a Varian Unity Inova-400 spectrophotometer operating at 400 MHz for ^{1}H NMR and 100 MHz for ^{13}C NMR. Column chromatography employed 230-450 mesh silica gel (Sorbent Technologies). TLC was performed on silica gel and visualization of spots was effected with UV light, potassium permanganate stain and/or ninhydrin stain. Commercial reagents were purchased from Aldrich and used as received unless otherwise noted. 8-Hexadecanol was purchased from Avocado Research Chemicals Ltd. (Heysham, Lancs, UK). Poly(ethylene glycol) (PEG) terminated with *N*-hydroxysuccinimidyl ester (NHS) and maleimide with MW of 3350 Da (NHS-PEG3350-MD) was purchased from Laysan Bio (Arab, AL). PEG terminated with monomethyl ether and mono(succinimidyl succinate) ester with MW of 1900 Da (PEG1900-SS) was purchased from Polysciences Inc. (Warrington, PA). PEG diamine with MW of 3350 Da (NH_2-PEG3350-NH_2) was purchased from Sigma (St. Louis, MO). PEG terminated with monomethyl ether and amine with MW of 2000 Da (PEG2000-NH_2) was purchased from Polymer Sources Inc. (Montreal, Canada). Reaction yields were not optimized.

Synthesis. Briefly, commercially available 8-hexadecanol was first activated by coupling with crosslinker 4-nitrophenyl chloroformate to afford **1**.[31] Reaction between **1** and NH_2-PEG3350-NH_2 gave the M-hexadecane-PEG3350-NH_2 molecule **2**, which was used to attach the M-hexadecane to substrate and AFM probe surfaces. The detailed synthesis procedure of **1** and **2** is included in the Supporting Information.

Chart *1*. Activated M-hexadecane **1** and M-hexadecane-PEG3350-NH_2 **2**.

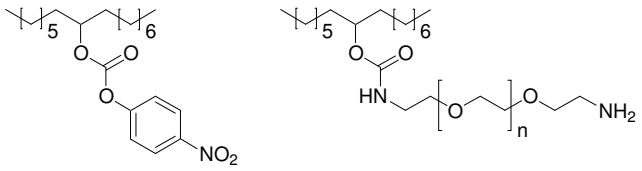

1 **2**

Sample Preparation. For each attachment configuration studied, two tip-sample pairs were separately prepared for measurement. A) End-attached hexadecane samples: Silicon nitride AFM cantilevers and substrate were cleaned in Piranha solution (1:3 hydrogen peroxide in sulfuric acid, by volume), rinsed with de-ionized water (DI, 18 MΩ·cm) and dried, transferred into a glove box under Ar, and subsequently aminated in a saturated ethanolamine hydrochloride solution in anhydrous DMSO for 48 h.[25,32] The cleaned and aminated cantilevers and substrate were first treated with a solution of 10 mg NHS-PEG3350-MD and 1 μL 1-hexadecanethiol in 525 μL anhydrous toluene/pyridine (20:1, by volume) for 24 h. A solution of 20 mg PEG1900-SS in 550 μL anhydrous toluene/pyridine (10:1, by volume) was added next and the reaction was kept running for another 48 h. Then a mixture of acetic anhydride/pyridine/anhydrous DMF (5:4:3, by volume) was added, and the cantilevers and substrate were passivated for at least 1 h and rinsed with DMF. The cantilevers and substrate were removed from the glove box and immersed in DI water of 50-60 ^{o}C for 20 min, and cleaned successively in toluene, DMF and ethanol for 5 min each on a platform shaker (for cantilevers) or sonicator (for substrate). Finally, the cantilevers and substrate were blown dry with UHP N_2 (National Welders Supply) and used immediately for data collection. B) Middle-attached hexadecane samples: Cantilevers and substrate were cleaned in 2% Hellmanex II (Hellma GmbH & Co KG, Müllheim, Germany) aqueous solution, rinsed with DI water and dried, transferred into glove box under Ar, and aminated as described above.[25,32] The cleaned and aminated cantilevers and substrate were first activated to become amino-reactive by treating with a solution of 50 mg of 1,4-phenylenediisothiocyanate (PDITC) in 1 mL anhydrous DMF/pyridine (10:1, by volume) for 4 h and rinsed thoroughly with DMF.[26,33] Next, they were treated with a solution of 10 mg of the synthesized M-hexadecane-PEG3350-NH_2 **2** in 0.6 mL anhydrous DMF/pyridine (10:1,

by volume) for 15 h. Then a solution of 15 mg of PEG2000-NH_2 in 0.3 mL anhydrous DMF/pyridine (9:1, by volume) was added, and the reaction was kept running for another 24 h. Finally, a solution of anhydrous DMF/ethanol amine (9:1, by volume) was added, and the cantilevers and substrate were passivated for 12 h and then rinsed thoroughly with DMF. The cantilevers and substrate were moved out of the glove box and cleaned in hexanes/i-propanol (3:2, by volume) at room temperature for 1 h. Then the cantilevers were rinsed with pre-heated hexanes/i-propanol. The substrate was boiled in hexanes/i-propanol for 15 min and rinsed with pre-heated hexanes/i-propanol for several times.[34] Both the cantilevers and the substrate were immersed in DI water of 50-60 ^{o}C for 20 min, and then cleaned successively in toluene, DMF and ethanol for 5 min each on a platform shaker (for cantilevers) or sonicator (for substrate). The cantilevers and substrate were blown dry with UHP N_2 and used immediately for data collection.

Data Collection and Manipulation. Force spectroscopy was carried out using an Asylum Research MFP-3D AFM. The cantilever spring constants were determined with the built-in thermal noise method.[35] The spring constants were 309, 170, 55 pN/nm for each of the three sets of MM, as well as 50, 58, 60, and 65 pN/nm for the two sets of EM and EE, respectively. Each cantilever was used for an entire set of probe velocities because the experimental error in determination of the spring constant might be ~20%.[36] The experimental procedure and the data processing were described previously.[24,25] All measurements were performed in 0.05 M pH 7 phosphate buffer at 25 ^{o}C. The probe was raster scanned over the substrate to obtain a good statistical average over the sample's surface. Force curves were collected with 5 nm relative trigger, 1 s surface dwell time, and probe velocity ranging from 0.3 to 5 μm/s. At each velocity, at least 4096 force curves were collected. Force–distance curves collected at each probe position were digitally stored for the subsequent analysis. Data processing and analysis was performed with software custom-written for Matlab.

II-c. Data Analysis. To distinguish rupture events between the tethered molecules from the ruptures between the tethered molecule and the substrate surface, the double tether approach was used.[24,25,29,37] Force-distance curves reveal that the rupture events occur at different probe positions above the sample

surface. The force curves with tether contour length corresponding to approximately twice the tether length (single tether length is ~30 nm, based on previously published mass-spectroscopy results)[24] were selected for subsequent analysis. The identified individual rupture events were fit with an extended freely jointed chain (FJC) model[38] to extract the apparent loading rates, tether Kuhn and contour lengths,[39] as described previously.[25,27,37] These values were used to account for the effects of the tether dynamics. The rupture forces measured at different probe velocities were binned into histograms with equal bin widths for further analysis.

II-e. Direct Histogram Fit to Force Probability Distribution. As shown previously, the collected force histograms for each set (eg. end-attached vs. end-attached) are fit by the two-bond rupture model to account for the shape of the probability distribution. [21,22,28,40] The probability density of the bond rupture p as a function of loading force F can be calculated according to [1,41] :

$$p(F) = -\frac{\mathrm{d}s(F)}{\mathrm{d}F} = \frac{k(F)}{v_F(F)} \cdot s(F) \qquad (1)$$

Here $s(F)$ is the bond survival probability, $k(F)$ is the force-dependent dissociation rate and $v_F(F)$ is the loading rate $v_F = \mathrm{d}F/\mathrm{d}t$. The dissociation rate k dependence on force can be described by different models of intermolecular potentials [21,30,42-46] and the loading rate depends on the pulling velocity, spring constant of the force sensor, and on tether dynamics.[38,47,48]

In AFM measurements, molecules are picked at random and it is possible to form more than one molecular bond during one tip-sample contact. The two-bond rupture model considers contribution from two simultaneous bond ruptures to the distribution of measured rupture forces. Because of possible variation in the polymer length, attachment point, and pulling angle, the relative difference between the first and second tether lengths, $\delta L_c = (L_{c,2} - L_{c,1})/ L_{c,1}$ is not controlled in the experiments. As the cantilever retracts, the force on the first tether (F_1) may differ from the force on the second tether (F_2) because of the difference in length. If the relative difference in length is at or below δL_{max}, then the

ruptures of the individual bonds will appear simultaneous in the AFM measurement, giving rise to the rupture events that can be approximately described by the probability distribution derived earlier: [28]

$$\Pi(F) \simeq (1+2\delta L_{max}) \cdot s(F/2) \cdot \left[s(F_2) - s(F_1) \right] / (F_1 - F_2) \qquad (2)$$

Here F is the experimentally measured total force acting on the cantilever: $F = F_1 + F_2$. Forces F_1 and F_2 along the individual tethers can be calculated by using tether dynamics models.[28] The histograms of rupture forces include both single and multiple bond rupture events. Therefore the resulting distribution function to fit the experimental data is:

$$P(F) = (1 - f_2)\, p(F) + f_2 \Pi(F) \qquad (3)$$

where f_2 is the relative fraction of two-bond rupture events in the data. Including the two-bond rupture in the histogram fitting requires two additional parameters: the maximum relative difference in tether lengths δL_{max} and the fraction of two-bond events f_2. The first of these parameters determines the position of the high force shoulder and the second parameter determines the amplitude of the two-bond ruptures. Although rupture of more than two bonds are possible, only two-bond ruptures are considered here because of the low grafting density used in our experiments [26,32] and for simplicity in the derivations of the analytical Eq. 2.

The measured histograms of rupture forces were fit directly with Eq. 3. Two sets of data with separately prepared tips and samples were fit simultaneously for each interaction pair to the same values of kinetic parameters and the maximum relative difference in the length of tethers δL_{max}. The amplitude f_2 was fit individually for each histogram to account for the probable difference in encountering of two-bond rupture events. Two models for the pmf are considered: the Bell-Evans model (corresponds to a triangular shaped potential) [49] and the parabolic potential with a sharp cusp model [30] (called cusp potential model for brevity). These models have been shown previously to yield the lowest and highest values of fitted kinetic parameters.[26,50] The cusp potential model explicitly uses the activation energy $\Delta G^{\ddagger}$.[30] In earlier work it was noted that the fit errors for k_0 are different in the direction of decreasing

and increasing of k_0,[51] indicating that the fit error function near the minimum is highly asymmetric along the k_0 coordinate. Therefore the activation energy $\Delta G^{\ddagger}$ was used as a fit parameter and in equations k_0 was replaced using $k_0 = A\exp\left(-\Delta G^{\ddagger}/k_B T\right)$ where A is the Arrhenius prefactor. The prefactor A was initially kept at 10^7 s^{-1}, as previously,[25,27,51] and variation of the prefactor values is considered below.

Limited force sensitivity is accounted for with a window function. The position of the window function was set to five standard deviations of the force RMS noise measured using the off-surface parts of the force curves, and the width of the rising edge of the window was held equal to the force RMS noise value. The expected histograms were calculated using eq 3 and the guessed fit parameters. The fitting minimizes the average RMS error between the measured and calculated histograms by adjusting the fit parameters using the Nelder-Mead direct search method included in the Matlab software.

In addition to including the high forces in the distribution, this fitting procedure accounts for the effects of tether anharmonicity by incorporating the eFJC polymer stretching model. Effects of the pmf shape are considered as well by using the cusp potential model in place of the Bell-Evans model.

Direct histogram fitting method is used here instead of more common most probable force analysis because previously was noticed that multiple bond ruptures might noticeably offset the most probable forces resulting in considerable variation in the determined kinetic parameters.[22,28]

III. Results

III-a. Force-separation plots. Figure 2 shows force separation plots for each of the interactions studied. The ruptures occurred at distances off the surface corresponding to approximately twice the length of the individual polymer tethers used in the covalent attachment of hexadecane to the surfaces. Prior to each rupture event, characteristic polymer stretching occurred. Each rupture event was fit with an extended FJC polymer-stretching model, to yield the contour length. Collected rupture events with contour lengths of less than 30 nm may correspond to other types of molecular events, and have been filtered out. This type of analysis is similar in practice to the unfolding of protein domains,[52] as the contour length is used as a "signature" of the desired molecular bond rupture events. Some of the curves

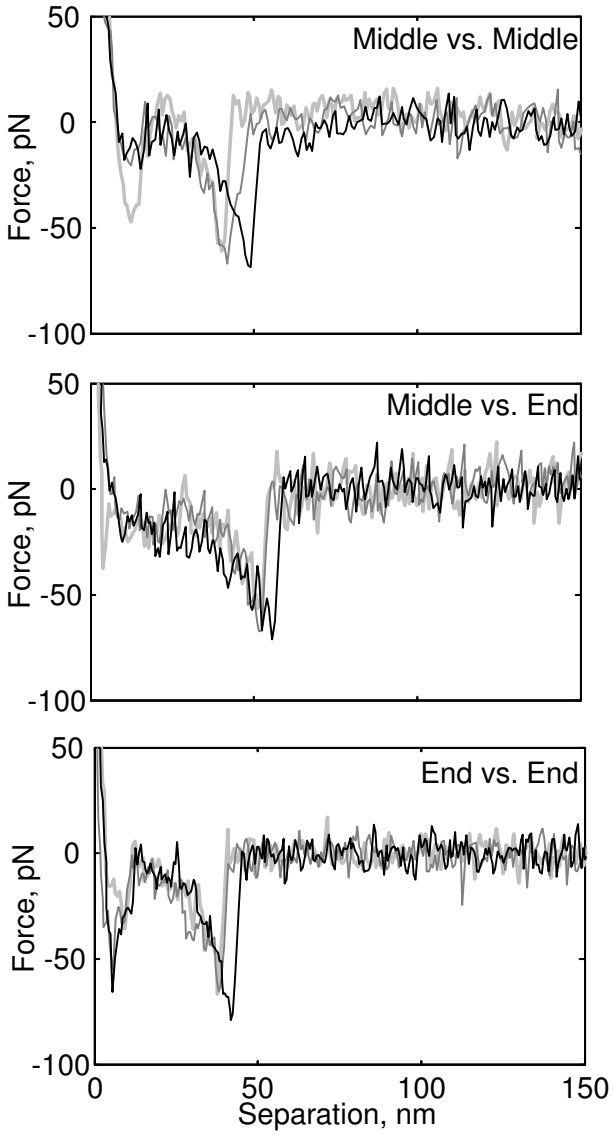

Figure 2. Representative force curves with double-tether rupture events are shown for each of the sets tested. The curves from both middle-attachment experiments were taken from the 1 μm/s probe velocity data sets, the symmetric end-attachment force curves were taken from the 700 nm/s probe velocity data set. The spring constants were 55 pN/nm, 58 pN/nm, and 60 pN/nm for the MM, ME, and EE curves shown here, respectively.

shown in Figure 2 have initial adhesion, but the polymer spacer mitigated this interference by moving the tested dimer by ~25 nm off the surface as illustrated in Figure 1. The ruptures are detected at ~50 nm tip-surface separation because tethers are used to attach molecules to tips and to substrates. The

consistent separation distance of the rupture event is a "signature" used to identify the desired molecular rupture events.

To further support the identification of rupture events as occurring between the molecules attached to the ends of the polymer tethers, an "empty tether" control experiment was performed. These experiments were performed exactly as the main experiments, using a fully functionalized AFM cantilever, but with a surface prepared with ethoxy-capped polymer tethers. The probability of detecting double-tether rupture events in this control experiment was found to be over an order of magnitude lower. This indicates that the vast majority of the measured rupture events corresponded to interactions between the hexadecane molecules attached to the polymer terminus.

III-c. Direct Histogram Fit to Force Probability Distribution. The two-bond model was simultaneously fit with the same kinetic parameters to the rupture force histograms for each interaction studied. The spring constants varied between these sets because the data resulted from separately prepared tips and surfaces. Fitting was performed on 3 sets of MM data each with 5 velocities, 2 sets of ME data with 5 velocities, and 2 sets of EE data with 4 velocities. Each set of velocities ranged from 300 nm/s to 5 μm/s. Figure 3 shows the histograms and probability density fits for one of the interactions. The other histograms and fits are available in the Supporting Information. The graph of the most probable force dependence on the apparent loading rate is not included because not all measured rupture forces come from rupture of single molecular bonds. Therefore the most probable forces may be shifted to higher values by presence of multiple bond ruptures. Consequently using the most probable force analysis might lead to systematic errors in derived parameters as we have shown in our previous publications. [22,28]

Each histogram shown in Figure 3, as well as in the figures in the Supporting Information, corresponds to data collected at a particular withdrawal speed (shown at the top of each histogram). The window function (dash-dotted line) and distribution fit (grey solid line), with the single-bond (grey dotted line) and two-bonds (black dotted line) components, are also shown in Figure 3. The fit lines for the Bell-Evans and cusp models are close within each data set, though the determined kinetic parameters

differ. Table 1 shows the determined kinetic parameters. The 95% confidence errors were found by bootstrapping. Note that the given errors in the kinetic parameters are similar to others in the field,[50] as well as authors own previous work.[24,25,27,51] The $\Delta G^{\ddagger}_{corr}$ column shows activated energies corrected by considering possible variations in the Arrhenius prefactor as explained below.

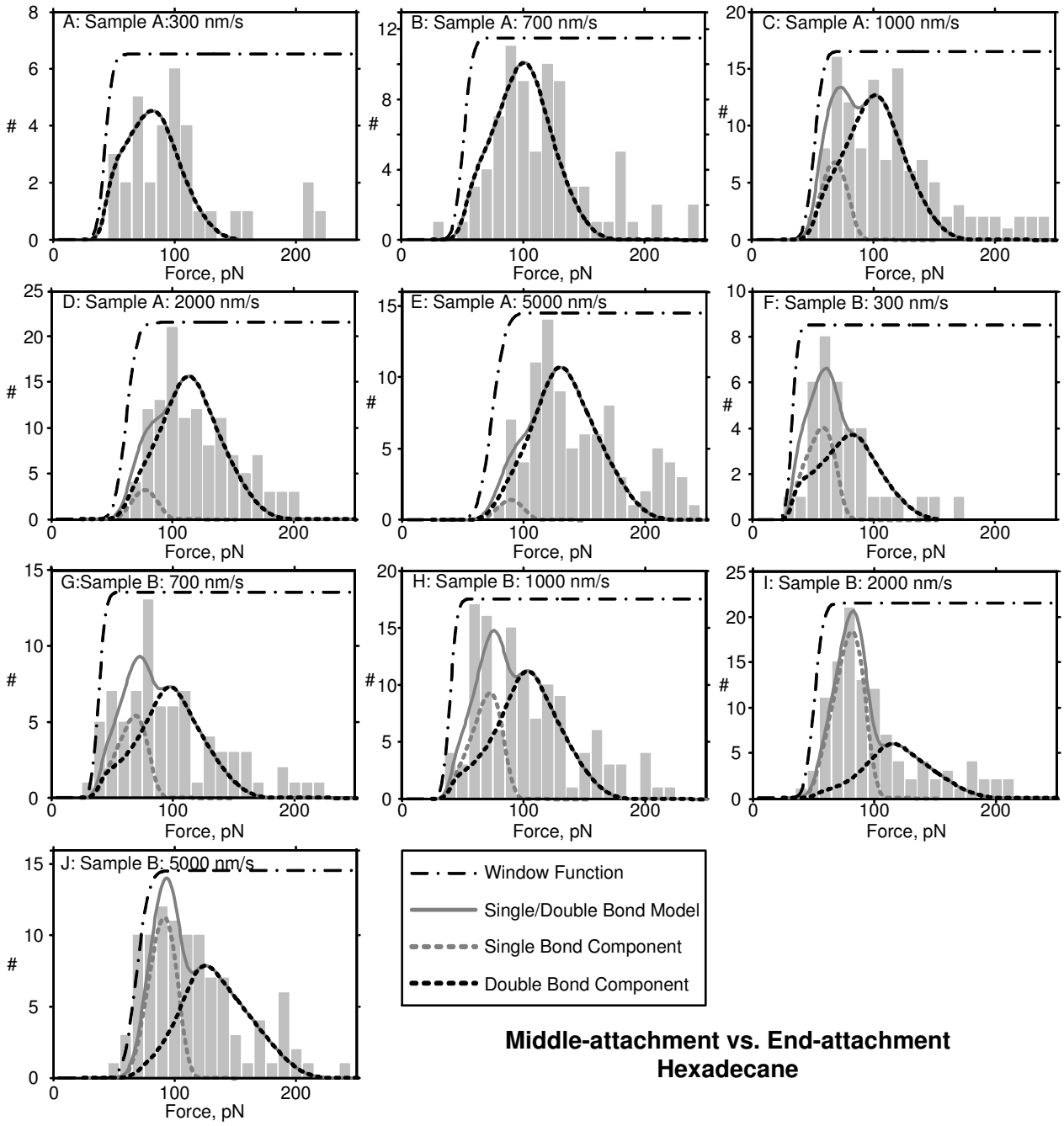

Figure 3. Panels A through J show the experimentally measured ME hexadecane rupture force histograms with the full distribution fits that use the Bell-Evans kinetic model. Panels A through E

correspond to one set of collected data, while Panels F through J correspond to a second set. The model better fits the second set of data because there are more data points to fit. The spring constants were 50 and 58 pN/nm for Samples A and B, respectively. Histograms and fits for the other attachment experiments are included in Supporting Information.

Table 1. Kinetic parameters determined with the Bell-Evans and cusp potential models

Model/Sample	$x^{\ddagger}$ (nm)	$\delta x^{\ddagger}$ (nm)	k_0 (1/s)	δk_0 (1/s)	$\Delta G^{\ddagger}$ (kJ/mol)	$\delta\Delta G^{\ddagger}$ (kJ/mol)	$\Delta G^{\ddagger}_{corr}$ (kJ/mol)
Bell Evans							
End vs. End	0.7	0.1	0.07	0.04	47	2	54
Middle vs. End	0.42	0.02	0.50	0.10	42	0.8	49
Middle vs. Middle	0.43	0.02	0.32	0.10	43	1	50
Cusp							
End vs. End	0.92	0.12	0.020	0.010	50	2	57
Middle vs. End	0.58	0.04	0.20	0.09	44	1.4	51
Middle vs. Middle	0.60	0.02	0.15	0.05	45	1	52

IV. Discussion

IV-a. Exponential Prefactor. Values of activation energy given in Table 1 depend on the Arrhenius prefactor A: increasing the prefactor by a factor of 10 increases the activation energy by approximately 5.7 kJ/mol. The exact value of the prefactor is unknown but can be estimated using physical models. The scaling of the prefactor can be considered similar to the scaling of the first-contact time between the ends in the diffusion-driven motion of the polymer chain. [53-55] The rate of the loop formation can be calculated using the modified theory of Schulten, Schulten and Szabo [55]

$$k_{loop} \approx \frac{24\sqrt{6}\,a\,D}{\pi N^2 b^3} = \frac{4\sqrt{6}\,a\,k_B T}{\pi^2 N^2 b^4 \eta} \qquad (4)$$

Here a is the capture distance for the ends of a chain, b is the Kuhn length, N is the number of Kuhn segments, and D is the diffusion coefficient. In the second equality $D = k_B T/(6\pi b\eta)$ is used where η is the viscosity. Because the measured $x^{\ddagger}$ is shorter than the Kuhn length of poly-(ethylene) (b = 1.4 nm) the capture distance was taken at the minimum physically meaningful value of b. The number of Kuhn segments and the Kuhn length was obtained from $b = C_n\, l /\cos(\theta/2)$ and $N = n\cos^2(\theta/2)/C_n$ where C_n is the characteristic ratio of 32-mer polyethylene, l is the carbon-carbon bond length, θ is the bond angle and n is the number of bonds in the chain.[56] Therefore

$$k_{loop} \approx \frac{4\sqrt{6}\, k_B T}{\pi^2 C_n \cos(\theta/2)\, n^2 l^3 \eta} \qquad (5)$$

Here the characteristic ratio C_n is less than the characteristic ratio of infinitely long poly-(ethylene) chain (7.4) and equals approximately to 6.1.[57] Using $\theta = 68°$, l = 0.154 nm, and η = 0.001 Pa·s gives $k_{loop} \approx 2\cdot 10^8$ s^{-1}. Water is a poor solvent for alkanes, this might further increase the prefactor; though for short chains (here $N \approx 3.6$) this increase is on the order of unity.[55] The calculated value of k_{loop} is noticeably higher than the prefactor used in the data analysis, therefore the activation energies are increased by 7 kJ/mol as shown in $\Delta G^{\ddagger}_{\text{corr}}$ column in Table 1. We note that this estimation of the pre-exponential factor does not include solvent degrees of freedom. However, if diffusion along solvent coordinate is slow[58] then multiple re-crossings of $x^{\ddagger}$ position along the one-dimensional pmf might occur during dissociation reaction.[59] Such re-crossings decrease the prefactor and correspondingly decrease the estimated $\Delta G^{\ddagger}$. To estimate significance of this effect we can compare characteristic time of motion along the solute coordinate given by $1/A \approx 5$ ns with the solvent dynamics of emptying the gap between hydrophobic solutes. Simulations of association of two hydrophobic spheres with radii of 1 nm indicate that characteristic time of bubble formation between the spheres is ~20 ps.[60] Therefore we expect that in dissociation of alkanes solvent contribution to the one-dimensional pmf is small.[58] Consequently the measured $\Delta G^{\ddagger}$ should be close to the activation energy of the dissociation reaction.

IV-b. Energy of the Transition State. The activation energy for hexadecane EE dissociation has previously been compared with the cavity model,[61] with a surprising agreement.[25,27] This agreement seems accidental because the cavity model calculates change in the free energy due to merging of two spherical empty cavities. Compensation between three disparate effects may account for the noted agreement. (1) The free energy of dimerization of cavities filled with hydrocarbons is expected to be lower than predicted by the cavity model because of the attractive interactions of water molecules with the non-polar solutes.[62] (2) The cavity models used previously assume spherical geometry of solutes. Possible conformational changes of interacting molecules during dimerization [22] are not accounted for in these models. (3) The activation energy of dissociation is obtained from force spectroscopy measurements, which may differ from the free energy of dissociation. For simple pmfs with one energy barrier [40] this energy should be larger than the difference between free energies of separated and dimeric states. An activation barrier is often predicted by simulations of hydrophobic interactions. The predicted height of the activation barrier for small methane-like particles and small alkanes (up to neopentane) is ~1-2 kJ/mol.[9,13-15,17,18] A significantly higher activation barrier (~8 kJ/mol) has been predicted for a pair of pre-formed Ala_{20} helixes in water. For larger solutes such as pre-formed Leu_{20} helixes, hydrophobic particles with radius of 1 nm and other simple geometric shapes, dimerization is predicted to have no activation barrier.[20,60,63,64]

The free energy of the transition state can be obtained as $G^{\ddagger} = \Delta G_{\mathrm{d}} + \Delta G^{\ddagger}$ where ΔG_{d} is the free energy of dimerization. The free energy of dimerization can be estimated as $\Delta G_{\mathrm{d}} = \gamma \Delta A$ where γ is the surface energy density and ΔA is the change in the solvent-accessible surface area.[62] Surface energy density for alkanes transferred from oil phase to water was estimated as γ = 17 $\mathrm{kJ \cdot mol^{-1} \cdot nm^{-2}}$. [65] The same value can be obtained from the Lum-Chandler-Weeks theory applied to alkane solutes in water for a solute with radius equal to the excluded solvent radius of a sphere that has the same volume as hexadecane.[66]

Change in the surface area upon dimerization depends on the geometry of molecules in the monomer and dimer states. Because these geometries have not been studied by molecular simulations, we consider first four primitive models of contact between two hydrophobic objects with spherical and cylindrical geometries as illustrated in Figure 4. Spherical geometry represents a collapsed state with volume of a sphere equal to the van der Waals volume of hexadecane. The radius of hexadecane in spherical geometry was calculated by the Carnahan-Starling van der Waals equation of state and is R = 0.41 nm.[67] The same result was obtained by calculating the hexadecane molecular volume using the additivity scheme (V = 0.28 nm^3).[68] The solvent accessible surface area (SASA) of a sphere was calculated as $4\cdot\pi\cdot(R+\sigma/2)^2$ = 3.74 nm^2 where σ is the diameter of water (0.28 nm).[61] This SASA is considerably less than the SASA of hexadecane in all-trans conformation (6.06 nm^2) calculated by extrapolation of SASA of shorter alkanes.[10] The all-trans conformation of hexadecane is used here as one of possible extended conformations mainly because SASA of all-trans monomer can be easily estimated from results of Gallicchio et al.[10] In cylindrical geometry the extended molecule is represented by a cylinder with two hemispherical caps. The length of a cylinder equals to the extended length of hexadecane [69] and radius of a cylinder (R = 0.27 nm) is selected such that the cylinder with caps has the same SASA as extended hexadecane. Volume of one hexadecane in the cylindrical model is 0.44 nm^3, noticeably higher than the van der Waals volume of hexadecane. Molecular volumes of dimers in all models equal to the volume of a corresponding monomer multiplied by a factor of two. In this section we do not consider a mechanism of transition between monomeric and dimeric states; shapes shown in Figure 4 are only used to represent the initial and final configurations and estimate energy of dimerization. Sizes of the model shapes in monomeric and dimeric states, changes in the solvent accessible area and energy of dimerization are included in Figure 4.

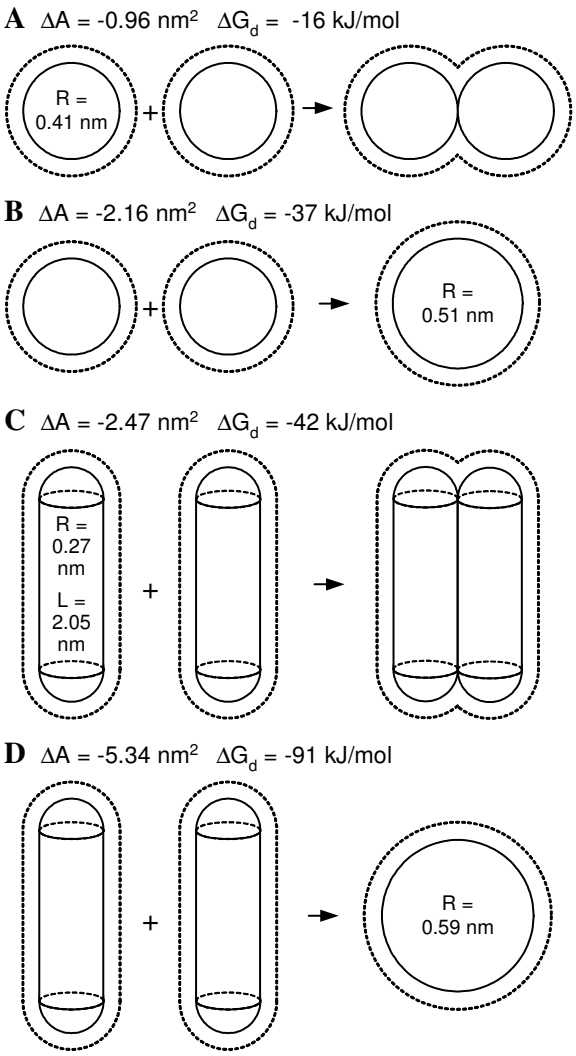

Figure 4. Four primitive schemes of hexadecane dimerization. Solid lines show molecular geometries and dashed lines illustrate the solvent excluded volumes.

For various reasons all of the geometrical schemes shown in Figure 4 are inconsistent with the presented experimental results. Here, the primitive models are considered based on the expected energies of the transition state; other aspects of these schemes will be considered below. In the touching spheres geometry (Figure 4A), the free energy of the transition state would be unphysically high (>35 kJ/mol) in comparison to the energy of the dimer state. Merging spheres (Figure 4B) would have activation energy of ~15 kJ/mol. Although this energy is higher than the transition state energy calculated for rigid hydrophobic molecules, it may correspond to the activation energy of *trans* → *gauche* transition.[15,70,71] The touching cylinders geometry (Figure 4C) would correspond to a smaller

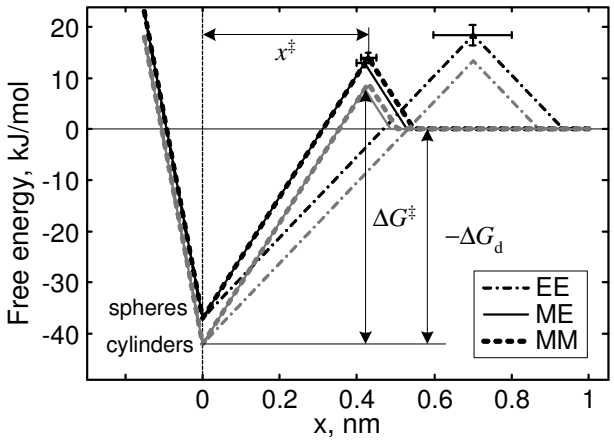

Figure 5. Schematic cartoon of the potential of mean force for dissociation of hexadecane dimer in water for three attachment configurations: EE – both molecules are attached at the end; ME – one molecule is attached in the middle and another at the end; MM – both molecules are attached in the middle. Black lines correspond to the merging spheres model (Figure 4B) and gray lines correspond to the touching cylinders model (Figure 4C).

transition state energy (~10 kJ/mol) than the merging spheres geometry and in this regard also represents a feasible scheme of dimerization. The transition state energy of two cylinders merging into a sphere (Figure 4D) would be very negative (< -35 kJ/mol), an unlikely scenario. Schemes B and C remain feasible, and are considered further below.

Cartoons illustrating relative positions of the transition states along the pulling coordinate that correspond to schemes B and C discussed above are shown in Figure 5. In these cartoons, zero distance corresponds to the pulling coordinate at the equilibrium dimer state. Possible energy landscape roughness and curvature are neglected. Also, the cartoon assumes that the free energy of the dimer state does not depend on the attachment point. However, the critical micelle concentration (cmc) for alkyl ethoxides with the same length of PEG chain is higher when the PEG chain is attached in the middle of alkyl chain.[72-74] Therefore it might be expected that the free energy of a hexadecane dimer with the PEG linker attached in the middle of the molecule is more positive than for the terminal attachment of the linker. (This effect indicates how the linker attachment that is necessary to perform the experiment

perturbs the experimental system.) Using the cmc predictor by Katritzky et al. [74] the difference between free energy of micelle formation between linear and branched hexadecane is expected to be approximately 3-5 kJ/mol. Therefore free energy corresponding to ME and MM configuration might be increased by a few kJ/mol. This correction makes energies of the transition state for different attachment configurations nearly the same.

IV-c. Anisotropy of Molecular Interaction. There is a remarkable variation between the barrier widths $x^{\ddagger}$ for different tether attachment geometries as shown in Table 1 and Figure 5. Larger barrier width $x^{\ddagger}$ for the symmetric EE configuration implies that in this configuration the attachment points in the dimer are displaced over larger distance prior to reaching the transition state than in other configurations. This difference is translated into a difference between stiffness of the molecular bond for different attachment geometries. Stiffness of molecular bonds can be estimated using the cusp potential model [43] as $k_m = 2\Delta G^{\ddagger} \Big/ \left(x^{\ddagger}\right)^2$. For EE, ME and MM arrangements this gives stiffness of 0.21±0.05, 0.47±0.06, and 0.45±0.03 N/m, respectively. We note that these stiffness values are obtained using a smooth potential model. If the actual energy landscape is rough the local stiffness at the bottom of the potential well might be higher than the stiffness calculated above. Stiffness of the polymeric tethers prior to rupture (measured to be approximately 0.01 N/m) was much lower than k_m. Therefore possible distortion of the molecular bond by the probe potential [75,76] was not considered in the data analysis. Measured attachment point dependencies of $x^{\ddagger}$ and bond stiffness contradict isotropic models that use a spherical shape of monomers (Figure 4A-B).

Measurements of solubility, [77,78] theoretical calculations [79,80] and recent force spectroscopy measurements [22] indicate that individual hexadecane molecules are likely to be in an extended (non-globular) conformation. Experiments comparing the compressibility of Langmuir films of 1-hexadecanoic acid (1-HDA) and 8-hexadecanoic acid (8-HDA) on water show that at surface pressure of ~18 mN/m the surface area of one 8-HDA molecule is ~2.8 times larger than the surface area of one 1-HDA.[81] If the conformation of 8-HDA were collapsed with the two alkane "arms" joined together then

the increase should be less than twice the 1-HDA values. This observation indicates that the linker attachment in the middle of hexadecane does not significantly alter the extended conformation of the monomer. Therefore observed variations in $x^{\ddagger}$ (Table 1) can be interpreted as anisotropy of molecular bond in respect to pulling direction.

Recent force spectroscopy measurements of interactions between linear alkane molecules with different sizes indicate that upon dimerization in water at room temperature alkanes shorter than octadecane undergo conformational transition from extended to collapsed state as sketched in Figure 4D. [22] However, as indicated above (section IV-b) this scheme is inconsistent with the measured activation energy. In addition, this geometry suggests that upon transition from collapsed to extended conformation distance between the end attachment points increases by ~1.4 nm, considerably exceeding the measured $x_{EE}^{\ddagger}$ (0.7-0.9 nm). This deficiency is a consequence of the absence of a molecular structure in primitive geometrical models. A simple model of a hexadecane molecule capable of conformational changes is a model of beads on a string. Hexadecane has approximately three Kuhn segments, [56,57] therefore four beads were selected to represent each molecule. The radius of beads was selected to preserve the length of stretched hexadecane L and the hexadecane SASA (A_{SA}). The hardcore radius of the bead equals to $R_b = A_{SA}/(2\pi(L+\sigma_w)) - \sigma_w/2$ where σ_w is a diameter of water molecule. It is interesting to note that this formula is independent of the number of beads and is accurate as long as there is overlap between solvation spheres of the beads. By assuming all-trans conformation of the extended hexadecane and extrapolating previously calculated [10] alkane SASAs the bead radius R_b equals to 0.274 nm.

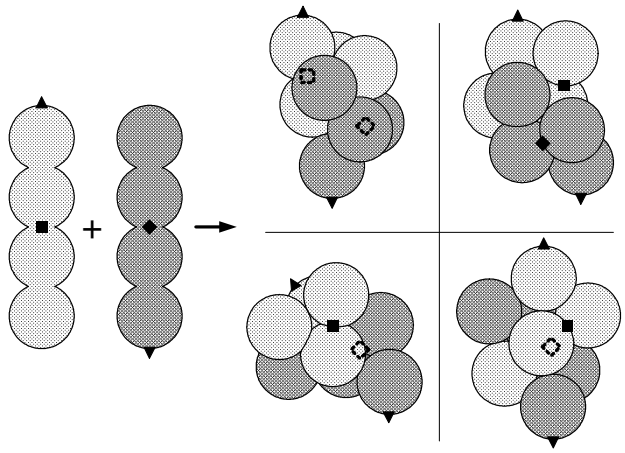

Figure 6. Possible geometries of hexadecane dimers using a four-beads model of hexadecane. Transition to a collapsed conformation occurs in the dimer state. The end attachments of the linkers are labeled with black triangles; the middle point on one molecule is labeled with a black square and on another with a black rhombus.

Several close-packed geometries representing the dimer state were generated. Four sample geometries are shown in Figure 6. The solvent accessible surface area of dimers was calculated using the analytical approach of Connolly by considering the overlapping spheres with radius of (R_b+σ_w/2). [82] The bead model predicts that transition from separated hexadecanes to the collapsed dimer produces change in the SASA of ~5.0±0.1 nm^2. Similar change in the SASA was calculated when a three-bead model was used to represent a collapsed hexadecane dimer. However, in the three-bead model distance between centers of contacting beads from different molecules in the dimer is less than the bond length. This makes the three-bead hexadecane model unphysical, and is why we chose to use four beads instead.

Surface free energy density that was used above (γ= 17 kJ·mol^{-1}·nm^{-2}) gives dimerization energy of ΔG_d = -85 kJ/mol. The absolute value of this energy is considerably larger than the measured activation energy resulting in a negative value of the free energy of the transition state. However, theoretical predictions indicate that the surface free energy density depends on the radius of solute.[11,12,83] For alkane-like beads with the solvent-excluded radius of 0.41 nm it is theoretically predicted that γ= 12

kJ·mol^{-1}·nm^{-2} and therefore the dimerization energy would be ΔG_d = -60 kJ/mol. [66] This value implies that activation barrier for dimerization of hexadecane is small or even absent.

The transition from a collapsed dimer state to the extended separated monomers state changes the distance between the attachment points. To estimate these changes it was assumed that in the transition state monomers are arranged parallel to each other with a gap equal to the diameter of water molecule. Differences in separation between the attachment points averaged for several different collapsed geometries for EE, ME and MM pulling geometries were found to be 0.70±0.10, 0.35±0.11, and 0.28±0.12 nm, respectively. Thus this bead model predicts that $x^{\ddagger}$ for EE pulling configuration should be larger than for ME and MM configurations by ~0.4±0.1 nm. From Table 1 the measured differences ($x^{\ddagger}_{EE}$ - $x^{\ddagger}_{ME}$) and ($x^{\ddagger}_{EE}$ - $x^{\ddagger}_{MM}$) are both ~0.3±0.1 nm. This agreement is remarkable given the simplicity of the model and supports explanation of the measured pulling direction anisotropy by conformational transition in the hexadecane monomers during dissociation of the dimer by pulling force.

V. Conclusions

The pulling coordinate dependence on hexadecane dimer dissociation has been studied in aqueous solution with three distinct configurations: end-attached vs. end-attached (EE), middle-attached vs. end-attached (ME), and middle-attached vs. middle-attached (MM). Careful data analysis yielded barrier widths ($x^{\ddagger}$) and activation energies ($\Delta G^{\ddagger}$) for each of these pairings, accounting for possible systematic errors. The barrier widths and activation energies were similar for the MM and ME configurations, while the barrier width was significantly longer (by 0.3 nm) and the activation energy slightly larger (by ~4 kJ/mol) for EE configuration. Detailed analysis indicates that the free energy of the transition state $G^{\ddagger}$ is likely to be similar (within k_BT) for all configurations.

Molecular dynamics simulations for these molecular systems are unavailable, so the results are compared with primitive geometrical models and a flexible four-bead model for hexadecane. The primitive dimerization schemes are unable to reproduce the measured anisotropy in $x^{\ddagger}$. The four-bead model predictions of the conformational changes in the dimer prior to dissociation match the measured

$x^{\ddagger}$ anisotropy. The SASA-based predictions of the free energy of dimerization require using the size dependent surface free energy for the free energy of the transition state to be larger than zero. The barrier-less association of hexadecanes in the four-bead model corresponds to the surface free energy of ~11 $kJ \cdot mol^{-1} \cdot nm^{-2}$ that agrees with the theoretically predicted value of ~12 $kJ \cdot mol^{-1} \cdot nm^{-2}$. [66]

Although the models considered here are basic, more sophisticated molecular models should not only reproduce the measured activation energy but also provide explanation of dissociation that is consistent with the measured anisotropy in the distance to the transition state.

Acknowledgment. The authors thank Duke University and NSF grant CHE-0719043 for financial support. The authors also gratefully acknowledge financial support from the ARO (W911NF-04-100191) and Gilbert Walker.

Supporting Information Available. Detailed description of the data manipulation as well as all histograms of rupture forces and loading rates are provided. This material is available free of charge via the Internet at http://pubs.acs.org.

VI. References.

(1) Evans, E.; Ritchie, K. *Biophys. J.* **1997**, *72*, 1541.
(2) Evans, E. *Faraday Discuss.* **1998**, *111*, 1.
(3) Dietz, H.; Berkemeier, F.; Bertz, M.; Rief, M. *Proc. Natl. Acad. Sci. U. S. A.* **2006**, *103*, 12724.
(4) Toofanny, R. D.; Williams, P. M. *J. Mol. Graph.* **2006**, *24*, 396.
(5) Kumar, S.; Giri, D. *Phys. Rev. Lett.* **2007**, *98*, 048101.
(6) Best, R. B.; Paci, E.; Hummer, G.; Dudko, O. K. *J. Phys. Chem. B* **2008**, *112*, 5968.
(7) Wallqvist, A.; Berne, B. J. *J. Phys. Chem.* **1995**, *99*, 2893.
(8) Wallqvist, A.; Berne, B. J. *J. Phys. Chem.* **1995**, *99*, 2885.
(9) Garde, S.; Hummer, G.; Paulaitis, M. E. *Faraday Discuss.* **1996**, *103*, 125.
(10) Gallicchio, E.; Kubo, M. M.; Levy, R. M. *J. Phys. Chem. B* **2000**, *104*, 6271.
(11) Chandler, D. *Nature* **2005**, *437*, 640.
(12) Ashbaugh, H. S.; Pratt, L. R. *Rev. Mod. Phys.* **2006**, *78*, 159.
(13) Sobolewski, E.; Makowski, M.; Czaplewski, C.; Liwo, A.; Oldziej, S.; Scheraga, H. A. *J. Phys. Chem. B* **2007**, *111*, 10765.
(14) Pratt, L. R.; Chandler, D. *J. Chem. Phys.* **1977**, *67*, 3683.
(15) Hummer, G.; Garde, S.; Garcia, A. E.; Paulaitis, M. E.; Pratt, L. R. *J. Phys. Chem. B* **1998**, *102*, 10469.
(16) Huang, X.; Margulis, C. J.; Berne, B. J. *J. Phys. Chem. B* **2003**, *107*, 11742.
(17) Czaplewski, C.; Kalinowski, S.; Liwo, A.; Scheraga, H. A. *Mol. Phys.* **2005**, *103*, 3153.
(18) Trzesniak, D.; Kunz, A. P. E.; van Gunsteren, W. F. *Chemphyschem* **2007**, *8*, 162.

(19) Zhou, R. H.; Huang, X. H.; Margulis, C. J.; Berne, B. J. *Science* **2004**, *305*, 1605.
(20) MacCallum, J. L.; Moghaddam, M. S.; Chan, H. S.; Tieleman, D. P. *Proc. Natl. Acad. Sci. U. S. A.* **2007**, *104*, 6206.
(21) Guo, S.; Ray, C.; Kirkpatrick, A.; Lad, N.; Akhremitchev, B. *Biophys. J.* **2008**, biophysj.108.133900.
(22) Ray, C.; Brown, J. R.; Kirkpatrick, A.; Akhremitchev, B. B. *J. Am. Chem. Soc.* **2008**, *130*, 10008–10018.
(23) Shimizu, S.; Chan, H. S. *Proteins* **2002**, *48*, 15.
(24) Ray, C.; Akhremitchev, B. B. *J. Am. Chem. Soc.* **2005**, *127*, 14739.
(25) Ray, C.; Brown, J. R.; Akhremitchev, B. B. *J. Phys. Chem. B* **2006**, *110*, 17578.
(26) Gu, C.; Ray, C.; Guo, S.; Akhremitchev, B. B. *J. Phys. Chem. C* **2007**, *111*, 12898.
(27) Ray, C.; Brown, J. R.; Akhremitchev, B. B. **2007**, *11*, 1963.
(28) Gu, C.; Kirkpatrick, A.; Ray, C.; Guo, S.; Akhremitchev, B. B. *J. Phys. Chem. C* **2008**, *112*, 5085.
(29) Ratto, T. V.; Langry, K. C.; Rudd, R. E.; Balhorn, R. L.; Allen, M. J.; McElfresh, M. W. *Biophys. J.* **2004**, *86*, 2430.
(30) Dudko, O. K.; Hummer, G.; Szabo, A. *Phys. Rev. Lett.* **2006**, *96*, 108101.
(31) Cai, T. B.; Lu, D.; Tang, X.; Zhang, Y.; Landerholm, M.; Wang, P. G. *J. Org. Chem.* **2005**, *70*, 3518.
(32) Riener, C. K.; Stroh, C. M.; Ebner, A.; Klampfl, C.; Gall, A. A.; Romanin, C.; Lyubchenko, Y. L.; Hinterdorfer, P.; Gruber, H. J. *Anal. Chim. Acta* **2003**, *479*, 59.
(33) Beier, M.; Hoheisel, J. D. *Nucl. Acids Res.* **1999**, *27*, 1970.
(34) Govender, S.; Jacobs, E. P.; Bredenkamp, M. W.; Swart, P. *J. Coll. Int. Sci.* **2005**, *282*, 306.
(35) Green, C. P.; Lioe, H.; Cleveland, J. P.; Proksch, R.; Mulvaney, P.; Sader, J. E. *Rev. Sci. Instrum.* **2004**, *75*, 1988.
(36) Proksch, R.; Schaffer, T. E.; Cleveland, J. P.; Callahan, R. C.; Viani, M. B. **2004**, *15*, 1344.
(37) Sulchek, T. A.; Friddle, R. W.; Langry, K. C.; Lau, E. Y.; Albrecht, H.; Ratto, T. V.; DeNardo, S. J.; Colvin, M. E.; Noy, A. *Proc. Natnl. Acad. Sci. U. S. A.* **2005**, *102*, 16638.
(38) Evans, E.; Ritchie, K. *Biophys. J.* **1999**, *76*, 2439.
(39) Oesterhelt, F.; Rief, M.; Gaub, H. E. *New J. Phys.* **1999**, *1*, 6.
(40) Guo, S.; Ray, C.; Kirkpatrick, A.; Lad, N.; Akhremitchev, B. *Biophys. J.* **2008**, biophysj.108.133900.
(41) Clandinin, M. T.; Cheema, S.; Field, C. J.; Garg, M. L.; Venkatraman, J.; Clandinin, T. R. *Faseb J.* **1991**, *5*, 2761.
(42) Dudko, O. K.; Filippov, A. E.; Klafter, J.; Urbakh, M. *Proc. Natl. Acad. Sci. U. S. A.* **2003**, *100*, 11378.
(43) Hummer, G.; Szabo, A. *Biophys. J.* **2003**, *85*, 5.
(44) Sheng, Y. J.; Jiang, S. Y.; Tsao, H. K. *J. Chem. Phys.* **2005**, *123*, 061106.
(45) Hanke, F.; Kreuzer, H. J. *Phys. Rev. E* **2006**, *74*, 031909.
(46) Hyeon, C.; Thirumalai, D. *J. Phys.-Condes. Matter* **2007**, *19*, 113101.
(47) Rief, M.; Fernandez, J. M.; Gaub, H. E. *Phys. Rev. Lett.* **1998**, *81*, 4764.
(48) Friedsam, C.; Wehle, A. K.; Kuhner, F.; Gaub, H. E. *J. Phys. Condens. Matter* **2003**, *15*, S1709.
(49) Schlierf, M.; Rief, M. *Biophys. J.* **2006**, *90*, L33.
(50) Hukkanen, E. J.; Wieland, J. A.; Gewirth, A.; Leckband, D. E.; Braatz, R. D. *Biophys. J.* **2005**, *89*, 3434.
(51) Ray, C.; Brown, J. R.; Akhremitchev, B. B. **2007**, *23*, 6076.
(52) Fisher, T. E.; Marszalek, P. E.; Fernandez, J. M. *Nat. Struct. Biol.* **2000**, *7*, 719.
(53) Pastor, R. W.; Zwanzig, R.; Szabo, A. *J. Chem. Phys.* **1996**, *105*, 3878.

(54) Chen, J. Z. Y.; Tsao, H. K.; Sheng, Y. J. *Phys. Rev. E* **2005**, *72*, 031804.
(55) Toan, N. M.; Morrison, G.; Hyeon, C.; Thirumalai, D. *J. Phys. Chem. B* **2008**, *112*, 6094.
(56) Rubinstein, M.; Colby, R. H. *Polymer Physics*; Oxford University Press: New York, 2003.
(57) Mattice, W. L.; Helfer, C. A.; Sokolov, A. P. *Macromolec.* **2003**, *36*, 9924.
(58) Berezhkovskii, A.; Szabo, A. *J. Chem. Phys.* **2005**, *122*, 014503.
(59) Geissler, P. L.; Dellago, C.; Chandler, D. *J. Phys. Chem. B* **1999**, *103*, 3706.
(60) Willard, A. P.; Chandler, D. *J. Phys. Chem. B* **2008**, *112*, 6187.
(61) Ben-Amotz, D. *J. Chem. Phys.* **2005**, *123*, 184504.
(62) Maibaum, L.; Chandler, D. *J. Phys. Chem. B* **2007**, *111*, 9025.
(63) Southall, N. T.; Dill, K. A. *Biophys. Chem.* **2002**, *101*, 295.
(64) Choudhury, N.; Pettitt, B. M. *J. Phys. Chem. B* **2006**, *110*, 8459.
(65) Brem, R.; Chan, H. S.; Dill, K. A. *J. Phys. Chem. B* **2000**, *104*, 7471.
(66) Huang, D. M.; Chandler, D. *J. Phys. Chem. B* **2002**, *106*, 2047.
(67) Ben-Amotz, D.; Herschbach, D. R. *J. Phys. Chem.* **1990**, *94*, 1038.
(68) Lepori, L.; Gianni, P. *J. Solut. Chem.* **2000**, *29*, 405.
(69) Tanford, C. *The Hydrophobic Effect: Formation of Micelles and Biological Membranes*; Wiley: New York, 1980.
(70) Mondello, M.; Grest, G. S.; Webb, E. B.; Peczak, P. *J. Chem. Phys.* **1998**, *109*, 798.
(71) Hafezi, M. J.; Sharif, F. *J Mol. Struct.* **2007**, *814*, 43.
(72) Elworthy, P. H.; Florence, A. T. *Kolloid-Z.-Z. Polym.* **1964**, *195*, 23.
(73) Corkill, J. M.; Goodman, J. F.; Harrold, S. P. *Trans. Faraday Soc.* **1964**, *60*, 202.
(74) Huibers, P. D. T.; Lobanov, V. S.; Katritzky, A. R.; Shah, D. O.; Karelson, M. *Langmuir* **1996**, *12*, 1462.
(75) Heymann, B.; Grubmuller, H. *Phys. Rev. Lett.* **2000**, *84*, 6126.
(76) Walton, E. B.; Lee, S.; Van Vliet, K. J. *Biophys. J.* **2008**, *94*, 2621–2630.
(77) Smith, R.; Tanford, C. *Proc. Natl. Acad. Sci. U. S. A.* **1973**, *70*, 289.
(78) Tolls, J.; van Dijk, J.; Verbruggen, E. J. M.; Hermens, J. L. M.; Loeprecht, B.; Schuurmann, G. *J. Phys. Chem. A* **2002**, *106*, 2760.
(79) Wallqvist, A.; Covell, D. G. *Biophys. J.* **1996**, *71*, 600.
(80) Mountain, R. D.; Thirumalai, D. *Proc. Natl. Acad. Sci. U. S. A.* **1998**, *95*, 8436.
(81) Dörfler, H. D.; Rettig, W. *Coll. Poly. Sci.* **1982**, *260*, 1126.
(82) Connolly, M. L. *J. App. Crys.* **1983**, *16*, 548.
(83) Graziano, G. *J. Phys. Chem. B* **2006**, *110*, 11421.